JOURNAL OF GEOPHYSICAL RESEARCH, VOL. 93, NO. B9, PAGES 10,149–10,162, SEPTEMBER 10, 1988

The Hydrothermal System at Newberry Volcano, Oregon

E. A. SAMMEL, S. E. INGEBRITSEN, AND R. H. MARINER

U.S. Geological Survey, Menlo Park, California

Results of recent geological and geophysical studies at Newberry Volcano have been incorporated into conceptual and numerical models of a magma-based hydrothermal system. Numerical simulations begin with emplacement of a small magma body, the presumed source of silicic eruptions at Newberry that began about 10,000 B.P., into a thermal regime representing 100,000 years of cooling of a large underlying intrusion. Simulated flow patterns and thermal histories for three sets of hypothetical permeability values are compatible with data from four geothermal drill holes on the volcano. Meteoric recharge cools the caldera-fill deposits, but thermal water moving up a central conduit representing a permeable volcanic vent produces temperatures close to those observed in drill holes within the caldera. Meteoric recharge from the caldera moves down the flanks and creates a near-isothermal zone that extends several hundred meters below the water table, producing temperature profiles similar to those observed in drill holes on the flanks. The temperatures observed in drill holes on the flanks are not influenced by the postulated Holocene magma body. The elevated temperature gradients measured in the lower portions of these holes may be related to the cumulative effect of older intrusions. The models also indicate that meteoric recharge to the deep hydrothermal system probably originates within or near the caldera. Relatively low fluid velocities at depth suggest that at least a significant fraction of the thermal fluid may be very old.

INTRODUCTION

The geological and geophysical studies reported in this issue and elsewhere have greatly advanced our knowledge of the evolution and structure of Newberry Volcano. An understanding of the hydrothermal system within the volcano is critical in current attempts to evaluate the potential for geothermal development at Newberry. The purpose of this paper is to examine previous studies that are relevant to the hydrologic system and to describe numerical models in which we attempted to simulate important aspects of the system.

On the basis of available evidence, we have assumed that a magma chamber exists at shallow crustal depths beneath the volcano and that parts of this chamber are now or were recently molten. Our objective was to develop a conceptual model of the hydrothermal system, incorporating the geophysical, geological, and chemical data and including a small magma chamber. The numerical simulations provided a means of exploring the general characteristics of the hydrothermal system. The data available from geophysical studies and test drilling provide few constraints on simulation models. Nevertheless, the numerical models described below are the basis for several tentative conclusions and hypotheses which should be of heuristic value.

GEOLOGIC BASIS FOR THE MODEL

The High Cascades region of Oregon (Figure 1) has been volcanically active for 9 m.y. or more and is locally characterized by long-lived accumulations of silicic magmas in the shallow crust. As a consequence of the long-continued volcanism, the region is now one of high heat flow. On the regional heat flow map of *Blackwell et al.* [1982], Newberry Volcano is within the region bounded by the 100 mW m^{-2} contour that includes the High Cascades (Figure 1).

Structural connections between Newberry and the High Cascades exist in the form of two major fault zones, the Walker Rim and the Sisters (Figure 1), that leave the Cascades trend and join alignments of volcanic vents to the southwest and northwest of Newberry [*MacLeod and Sherrod*, this issue]. Newberry may also represent the culmination of a westward progression of silicic volcanism trending across the Basin and Range Province in southern Oregon [*MacLeod et al.*, 1975]. Either of these two associations might be sufficient to explain the long-continued volcanism and the presence of significant volumes of silicic extrusive rocks at Newberry.

Geologic evidence presented by *MacLeod et al.* [1981, 1982] and *MacLeod and Sherrod* [this issue] indicates that Newberry Volcano has been intermittently active for more than 500,000 years but probably less than 700,000 years. Collapse of the summit to form a caldera probably began about 500,000 years ago and occurred in several episodes, leaving an outer ring of faults that nearly enclose the caldera, as well as an inner set of ring fractures in the southeastern quadrant of the caldera (Figure 2). The caldera is now partly filled with fragmental debris to a depth of about 500 m.

Following a long period of intermittent eruptive activity, during which large volumes of mafic magma cooled and solidified beneath the volcano, the most recent eruptive cycle began about 10,000 years B.P. [*MacLeod and Sherrod*, this issue]. Rocks extruded during this cycle range from basaltic andesite lava flows on the flanks to rhyolite flows and domes in the caldera (Figure 2) and on the southeast flank. The similar composition and physical characteristics of the rhyolites suggest that they erupted from a single magma chamber at near-solidus temperatures, with little crystallization during the entire eruptive cycle. Heat supplied by basaltic underplating during this period may have prevented crystallization of the silicic magma. Mafic lava flows, erupted in a concentric pattern during this same period, incorporate fragments of silicic magma. The absence of Holocene mafic rocks within the area bracketed by the Holocene rhyolites suggests the shadow effect of a shallow, centrally located silicic chamber [*MacLeod and Sherrod*, this issue].

There is no direct geologic evidence regarding depth to the magma chamber, but by analogy with other known volcanic systems containing highly evolved silicic magmas, the magma

Paper number 7B1038.
0148-0227/88/007B-1038$05.00

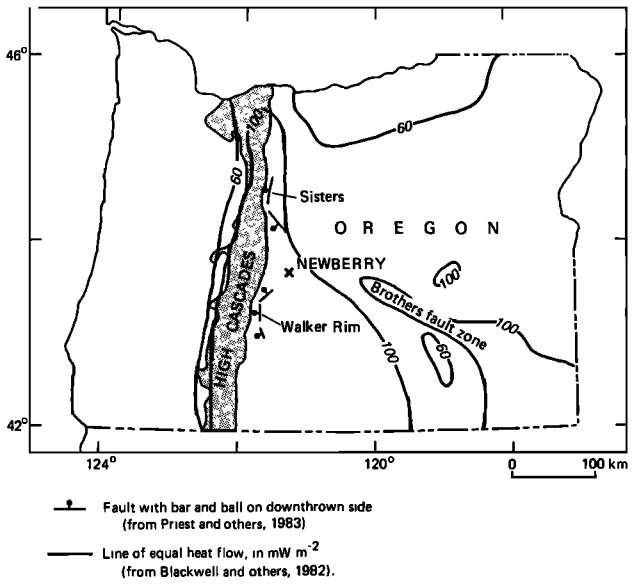

Fig. 1. Map of Oregon, showing the location of Newberry Volcano, the regional heat flow pattern, and major fault zones in the area around Newberry.

chamber at Newberry may be located at shallow crustal depths. Recent interpretations of seismic data suggest that a small body of magma exists at a depth of about 3 km below the caldera surface [*Achauer et al.*, this issue].

Test Drilling

Data from two intracaldera drill holes provide useful information on conditions at relatively shallow depths and afford insights into probable conditions at greater depths. Locations of these drill holes are given in Figure 2. U.S. Geological Survey (USGS) drill hole Newberry 2, cored to a depth of 932 m in the caldera in 1981, encountered temperatures of about 100°C at depths between 400 and 450 m and reached a temperature of 265°C at 930 m. A permeable, gas-bearing interval was encountered between 930 and 932 m [*Sammel*, 1981]. Rocks in the upper 500 m were predominantly permeable tuffs, tuff breccias, and sediments; the 500- to 930-m interval contained mainly lava flows and flow breccias [*MacLeod and Sammel*, 1982]. Below about 700 m, vertical permeability decreased significantly, although the interflow breccias still provided horizontal permeability. The permeability decrease was caused mainly by fracture filling and hydrothermal alteration [*Keith and Bargar*, this issue].

The second drill hole in the caldera, RDO-1 (Figure 2), was completed to a depth of 424 m by Sandia National Laboratories in 1983 [*Black et al.*, 1984]. Water temperatures encountered in the Sandia hole were significantly higher than those at comparable depths in Newberry 2. Temperature profiles from Newberry 2 and RDO-1 are compared with some of our model results in Figures 6 and 8 below. Data from three other drill holes, GEO N-1, GEO N-3 [*Swanberg et al.*, this issue], and USGS Newberry 1 [*MacLeod and Sammel*, 1982], provide some information about conditions on the flanks. (See Figure 2 for locations.) The temperature profile from GEO N-1 is included in Figure 6.

A 20-hour flow test of the Newberry 2 drill hole produced about 33,000 kg of fluid [*Ingebritsen et al.*, 1986]. The flow rate declined from the initial rate of about 0.8 kg s^{-1} to less than 0.3 kg s^{-1} during the course of the test. The mass ratio of liquid water to vapor was about 3:2 at the separator and stayed fairly constant throughout the test (Figure 3). For the first 8 hours of the flow test the vapor phase was about half steam and half CO_2 by weight. For the latter part of the test there are insufficient data to calculate the CO_2 content. Most of the produced fluid probably came from the 2-m-thick interval at the bottom of the hole.

The average enthalpy of the steam/water mixture at the separator was about 1200 kJ kg^{-1} (Figure 3). Because of the large temperature gradient into the surrounding rocks at early times and the low flow rate, heat loss from the wellbore was significant. A simple conductive model gives overall losses of about 1200 kJ per kilogram of H_2O produced, so that the average enthalpy of the H_2O at bottom-hole was at least 2400 kJ kg^{-1}, corresponding to a steam quality of about 70% at the bottom-hole temperature of 265°C. The actual heat loss per unit mass may have been even higher due to convective

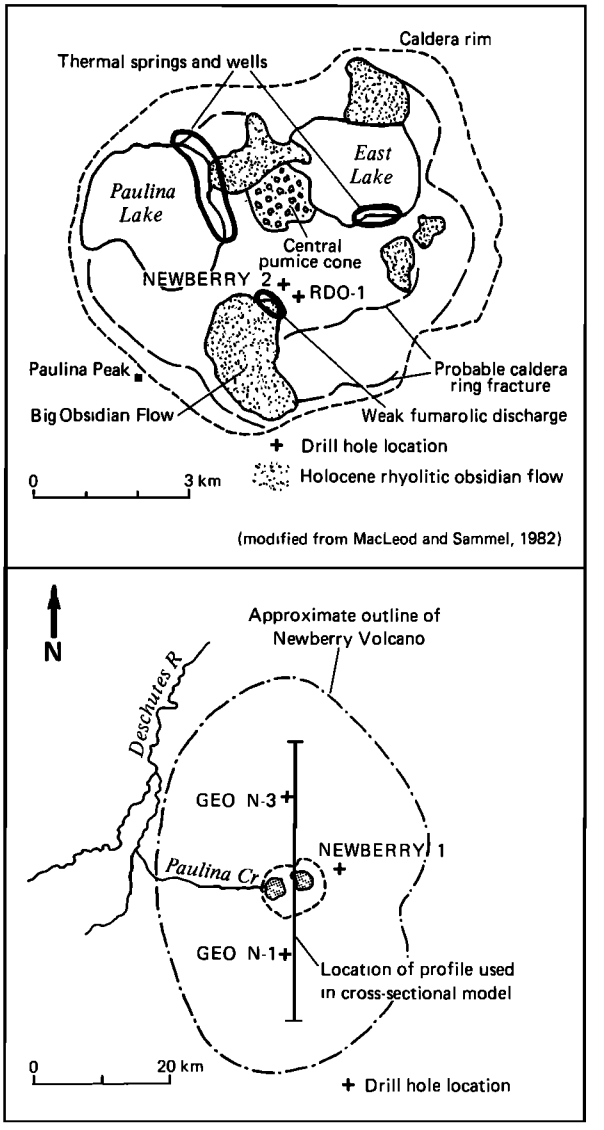

Fig. 2. Maps of (top) Newberry caldera and (bottom) Newberry Volcano, showing drill hole locations and other features discussed in the text.

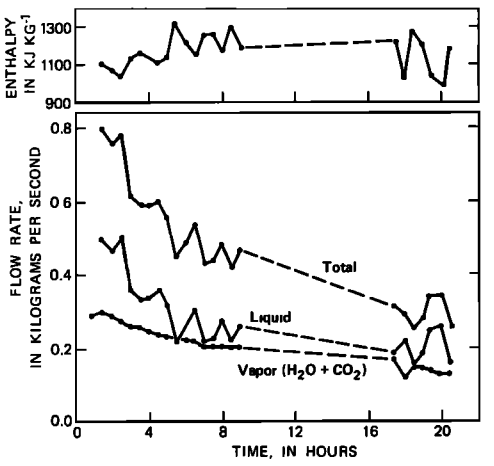

Fig. 3. Data from the flow test of Newberry 2. Flow rates were measured at a separator, and enthalpy was calculated on the basis of the temperature and steam quality at the separator [from *Ingebritsen et al.*, 1986].

effects, and it is likely that the fluid entering the bottom of the wellbore was largely or entirely steam and CO_2.

The high bottom-hole steam quality and the high CO_2 content of the produced fluids would be consistent with, but do not necessarily imply, two-phase (boiling) conditions in the formation prior to the flow test. Given sufficiently low matrix permeability, saturated or superheated steam can be produced even where liquid saturations approach 100% [*Pruess and Narasimhan*, 1982]. The high CO_2 content of the produced fluid (about 20 wt %) might be explained in terms of steam separation from a 265°C fluid with a relatively low (0.3 wt %) CO_2 content.

Hydrologic Studies

Only a small amount of thermal water rises to surface or near-surface levels in Newberry caldera. The total flow rate from thermal springs in and near the two lakes in the caldera (Figure 2) is probably no more than about 12 kg s^{-1} [*Sammel and Craig*, 1983]. There may be a significant subsurface flow of thermal water into the upper few hundred meters of caldera-fill deposits from ring fractures or volcanic vents, as indicated by the hot water encountered in the two caldera test holes [*Keith and Bargar*, this issue].

Thermal fluid (H_2O) sampled during the flow test of the Newberry 2 drill hole had an isotopic composition of about $\delta D = -100‰$ and $\delta^{18}O = -9.2‰$ [*Carothers et al.*, 1987]. Thermal water from hot springs and shallow (<25 m) domestic wells in the caldera may be a mixture of such thermal water (liquid or steam) of deep origin with cold water of the shallow groundwater system, which has an isotopic composition of about $\delta D = -115‰$ and $\delta^{18}O = -15.5$ [*Sammel and Craig*, 1983]. Chemically, the major dissolved constituents of the thermal spring waters are bicarbonate, sulfate, and sodium; carbon dioxide exsolves from the waters as they discharge. Weak fumarolic activity is localized along the toe of the Big Obsidian Flow and consists predominantly of carbon dioxide gas. No fluid from the high-temperature geothermal system in Newberry has been detected on the flanks of the volcano or in adjacent streams. However, thermal fluids as dilute as those that discharge in the caldera could easily emerge undetected in large streams such as the Deschutes River (Figure 2).

Annual precipitation within the caldera is about 890 mm. Estimates of stream discharge from the caldera, evapotranspiration, and evaporative losses from the lake surfaces suggest that about 180 mm of this total is available for recharge (approximately 250 kg s^{-1} or 5.7×10^{-6} kg s^{-1} m^{-2}). The estimate of recharge has a probable maximum error of about 50% [*Sammel and Craig*, 1983].

Precipitation on the flanks of the volcano is significantly less than in the caldera, and recharge through the flank rocks is probably small. Nevertheless, any precipitation that exceeds evapotranspiration on the flanks is absorbed; the only surface stream on the volcano is Paulina Creek (Figure 2), which issues from Paulina Lake and flows down the west flank of the volcano without a significant increase or decrease in flow [*Sammel and Craig*, 1983].

Conceptual Model of the Hydrologic System

The conceptual model on which the numerical models are based is essentially that proposed by *Sammel* [1983] and expanded on the basis of results from recent drilling and geophysical studies. The model supposes a high-level water table in the caldera, maintained by precipitation. Water in the caldera fill is heated by conduction from below as well as by small amounts of thermal fluid rising through fractures and volcanic vents. Below the relatively permeable caldera-fill deposits, at depths greater than about 500 m, permeabilities are extremely low in thick strata of lava flows and tuffs [*Keith and Bargar*, this issue]. These rocks form a generally tight confining layer that may overlie a zone of high-temperature convective flow at depths greater than 1 km. In limited areas near ring faults and volcanic vents, high vertical permeabilities allow exchange of fluid between the caldera fill and the deep high-temperature zone. Little of the meteoric water in the caldera fill makes its way directly downward. Most of the water flows laterally down the flanks of the volcano through permeable flow tops and basal breccias such as those observed in the GEO N-1 drill hole [*Swanberg et al.*, this issue] and the Newberry 1 drill hole [*MacLeod and Sammel*, 1982].

The source of heat that drives the present hydrothermal system is assumed to be a small mass of silicic magma that is located at or near the top of older cooled intrusions. The silicic magma has remained at temperatures above the solidus for most of the past 10,000 years. Depth to the top of the magma is assumed to be 3 km below the caldera floor.

Numerical Simulations

Both radial and cross-sectional models were constructed for the study. Each included a range of permeability cases. Eight hydrogeologic units were differentiated, including magma, basaltic flow rocks, caldera fill, and permeable vertical conduits. A water table at the caldera surface was represented by constant pressure/temperature nodes. Discharge from the model occurred across constant pressure/temperature boundaries at a radial distance of 20 km.

The numerical code used for the simulations was developed at the Lawrence Berkeley Laboratories by various workers over a period of several years and was put into its final form by *Bodvarsson* [1982]. The code, PT, employs an integrated finite-difference method for solving coupled equations of mass and energy transport. To describe fluid properties at temperatures up to 1000°C and pressures of up to 1000 bars, Ingebritsen modified the code using a bicubic spline interpolation on data read from the steam tables of *Keenan et al.* [1978].

Although the code is limited to single-phase fluid, it was chosen because of its flexibility in handling various boundary conditions, node geometries and connections, and physical properties of 10 different materials. A limitation of the code is the use of a constant specific heat capacity for the fluid. Except in the critical region, heat capacity varies only between about 3.0 and 6.4 kJ kg^{-1} K^{-1}; however, it increases dramatically in a narrow pressure-temperature range near the critical point. The computer code and its limitations with respect to the system considered are discussed further in the appendix.

Radial Models With Conductive Heat Flow

Early simulations used radial models, in which the center of symmetry was the center of the caldera and nodal volumes and connected areas at depth were those that would occur in a three-dimensional case. The first cases addressed the conductive cooling of magma bodies 2–3 km thick and 6–10 km in diameter at depths of 3 km and below. These bodies were generalized representations of the older intrusions, now at subsolidus temperatures, inferred from gravity and seismic data [*Griscom and Roberts*, 1983; *Williams and Finn*, 1985; *Stauber et al.*, this issue].

Details of the conductive simulations are omitted from this paper for the sake of brevity. However, we include a brief summary because the temperature distribution from one of the cases provided the initial temperature distribution for the convective cases described below.

Conductive heat flow in the volcano and underlying magma was simulated to depths of 6 km and a radial distance of 20 km. The distribution and magnitudes of material properties were the same as those used in later convective models, but permeability was uniformly zero. Ring dikes, modeled on the basis of gravity and seismic data [*Griscom and Roberts*, 1983; *Stauber et al.*, this issue], were emplaced at various times after initial plutonic intrusions.

The ring dikes are probably more than 100,000 years old (N. S. MacLeod, oral communication, 1985), and their thermal effects dissipated rapidly in the conductive models. These facts suggest that the ring dikes could have had no thermal effect on the Holocene hydrothermal system.

At simulation times greater than about 75,000 years, temperature distributions to depths of 3 km were very similar regardless of magma chamber size. The conduction-only solution from a representative radial model at a time of 100,000 years was used as the initial temperature distribution for convective models that are the subject of this paper.

Cross-Sectional Convective Model

Most of the convective models used the cross section shown in Figure 4*a*. The locations of test holes Newberry 2 (USGS), RDO-1 (Sandia), and GEO N-1 and N-3 (Geo Operator Corporation) are projected on this section for reference.

The cross section permitted departures from the symmetry imposed by the radial model, allowing features on one side of the volcano to differ from those on the other. For instance, there is a difference in water table elevation of about 90 m from south to north across the volcano, based on hydrologic data collected from wells situated on the outer flanks of the volcano and beyond (L. A. Chitwood, written communication, 1986), and from GEO N-1 and GEO N-3 (Figure 2) [*Swanberg et al.*, this issue]. The data from the two GEO Operator wells on the flanks of the volcano are remarkably consistent with the water table slope that was projected from the outer boundaries of the volcano on the basis of the Chitwood data.

The boundaries of the cross-sectional model were treated as indicated in Figure 4*a*. The upper boundary in the caldera is modeled as a constant pressure/temperature boundary at a pressure of 1 bar and a temperature of 1°C. It is fixed at an altitude of 1950 m above sea level, the approximate altitude of the lake surfaces in the caldera. Outside the caldera, the water table is also treated as a constant pressure/temperature boundary at a pressure of 1 bar, but vertical recharge on the flanks of the volcano is restricted by assigning low vertical permeability at this boundary in accordance with estimates of recharge discussed above. Where the water table elevation is unconstrained by drill hole data, it was positioned by interpolation. Initial temperatures at the water table boundary outside the caldera varied with depth below the land surface.

The lateral boundaries were treated as constant pressure/temperature boundaries having a hydrostatic pressure distribution and a temperature distribution derived from the early conduction-only runs with the radial model (Figure 4*b*). The lower boundary was treated as a no fluid flow, controlled heat flow boundary, with a conductive heat input of 105 mW m^{-2}, a reasonable rate for the area occupied by the volcano (Figure 1). The flow regime is divided into polyhedrons constructed by drawing perpendicular bisectors to lines connecting the 459 nodal points shown in Figure 4*a*.

Material and Fluid Properties

The cross-sectional model includes eight hydrogeologic units having differing thermal and hydraulic properties. Values of rock and fluid properties used in the model are given in Tables 1 and 2. The spatial distribution of the hydrogeologic units is shown in Figure 4 and subsequent figures.

Three sets of permeability values were used, representing low, intermediate, and high estimates for each hydrogeologic unit (Table 1). The values chosen fall within the range of field measurements in volcanic terrains reported in the literature, primarily those from *Brace* [1980, 1984], *Hardee* [1982], *Henley and Ellis* [1983], *Sammel* [1980], and *Sammel and Craig* [1981].

The relative magnitudes of permeabilities chosen for intracaldera hydrogeologic units to depths of a kilometer or more were strongly influenced by visual observations of drill core from Newberry 2 and RDO-1. The caldera-fill deposits (Figure 4*a*, FILL) are modeled as a uniformly permeable mass to a depth of 500 m; the ratio of vertical to horizontal permeability is small ($k_x/k_y = 0.1$). The extent of this unit was estimated partly on the basis of Schlumberger resistivity data, which showed generally uniform moderate resistivities within the caldera fill, and on transient electromagnetic soundings (TEM), which showed a transition to more conductive rocks at depths of 400–700 m [*Fitterman et al.*, this issue]. On the basis of these findings, interpretations of core from Newberry 2 [*Keith and Bargar*, this issue] were extrapolated to the entire caldera fill.

Beneath the caldera fill, the properties of units FLOW 4 and FLOW 5 are based on TEM and magnetotelluric (MT) data, which show low resistivities that are interpreted to result from alteration products in the rocks as well as from hot pore fluids [*Fitterman et al.*, this issue]. *Keith and Bargar* [this issue] point out that the drill core from Newberry 2 in the depth interval 500–930 m has extremely low vertical permeability which decreases with depth due to the presence of alteration minerals which fill veins and fissures. Horizontal

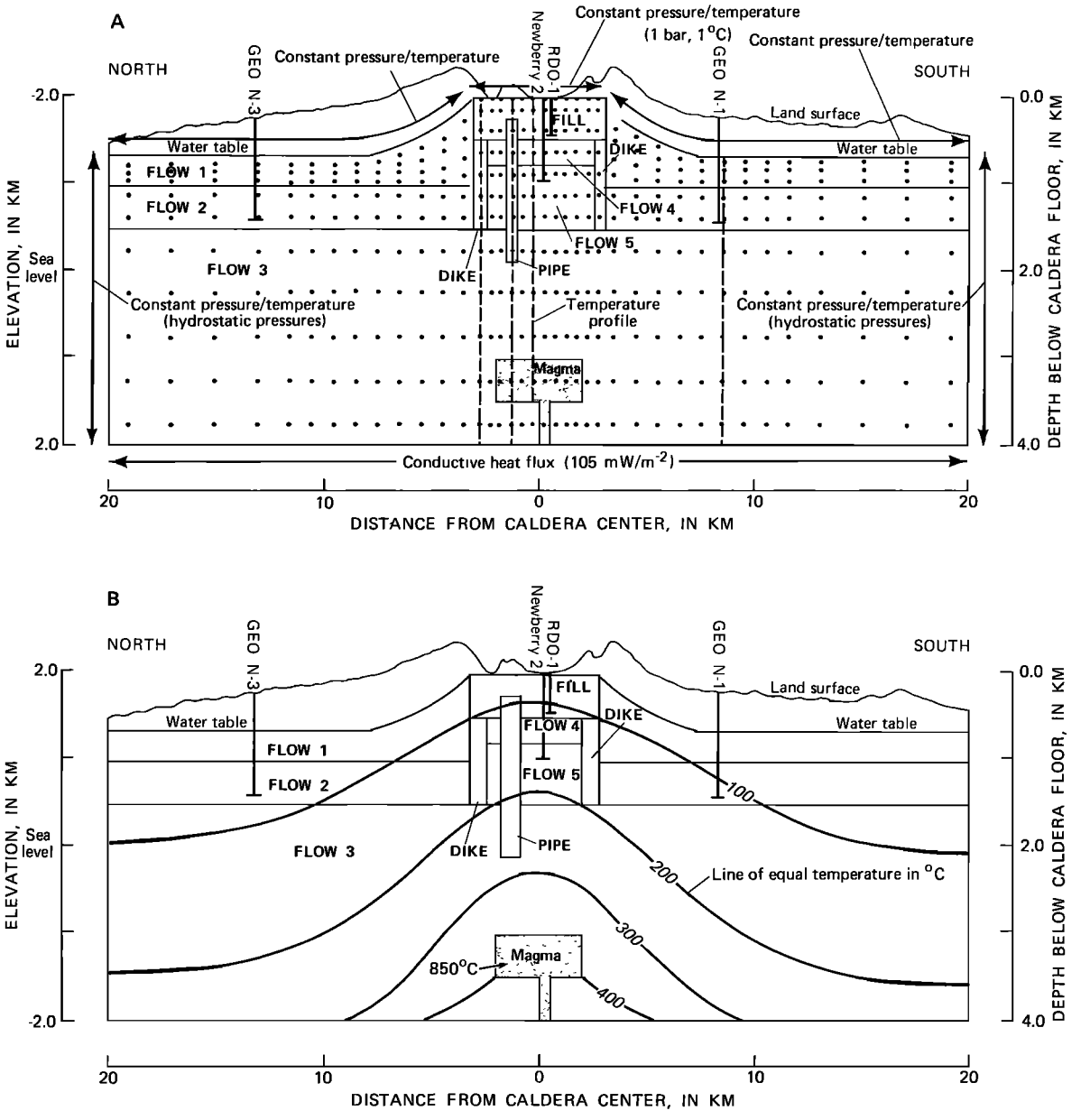

Fig. 4. (*a*) Geometry and boundary conditions used in the cross-sectional model. Dots show the positions of nodal points where pressure, temperature, fluid properties, and flow rates were calculated. Values of permeability and other rock properties assigned to the various hydrogeologic units are given in Tables 1 and 2. (*b*) Initial temperature distribution in the cross-sectional model. Initial pressures were hydrostatic. The initial temperature distribution is the solution from 100,000 years of conductive cooling of a 3-km thick, 10 km in diameter magma body emplaced in a radial model at 3-km depth.

permeabilities are somewhat higher in thin flow breccias and vesiculated tops of lava flows. These rocks form a generally tight cap over the hydrothermal convection system below. The depth to the base of the low permeability layers suggested by the MT data is between 1.5 and 2 km [*Fitterman et al.*, this issue]. We have used a depth of 1.5 km in the model.

The deepest hydrogeologic unit in the model, FLOW 3 (Figure 4), was given a permeability higher than that of FLOW 5 in all cases. In the absence of deep drill hole data, we relied on the electrical data which suggest that a high resistivity zone underlies the conductive layer described above. The resistive, probably less altered layer extends to depths below the bottom of the model [*Fitterman et al.*, this issue]. Although depths to the high-resistivity zone generally increase with distance from the caldera, the depth increase is not uniform around the volcano. For the sake of simplicity, the elevation of the top of this layer was kept constant in the model at 450 m above sea level. At the depth represented by the lower boundary of the model, approximately 2 km below sea level, the rocks may include Tertiary sedimentary rocks as well as volcanic rocks [*Wells and Peck*, 1961].

Beneath the flanks of the volcano, two upper layers, FLOW 1 and FLOW 2, were differentiated in order to provide for flexibility in experimentation. FLOW 1 was given permeabilities that, in some cases, equaled those in the FILL unit. FLOW 2 has lower permeabilities. It was possible to constrain the range of permeabilities in the upper flanks by numerical experimentation, since most of the 250 kg s^{-1} of recharge to

TABLE 1. Permeability Values Assigned to the Hydrogeologic Units

	Low-Permeability Case		Intermediate-Permeability Case		High-Permeability Case	
	k_x	k_z/k_x	k_x	k_z/k_x	k_x	k_z/k_x
FILL	1×10^{-14}	0.10	1×10^{-13}	0.10	5×10^{-12}	0.10
DIKES and PIPE	5×10^{-15}	5000.	5×10^{-15}	5000.	5×10^{-15}	5000.
FLOW 1	1×10^{-15}	0.10	1×10^{-13}	0.10	5×10^{-13}	0.10
FLOW 2	5×10^{-16}	0.05	5×10^{-15}	0.10	1×10^{-14}	0.10
FLOW 3	1×10^{-17}	0.01	1×10^{-16}	0.01	1×10^{-15}	0.05
FLOW 4	5×10^{-16}	0.05	1×10^{-15}	0.05	1×10^{-13}	0.10
FLOW 5	1×10^{-18}	0.01	1×10^{-17}	0.01	1×10^{-16}	0.01
MAGMA	1×10^{-18}	1.0	1×10^{-18}	1.0	1×10^{-18}	1.0

The hydrogeologic units are shown in Figure 4*a*. The permeabilities of the DIKES, PIPE, and MAGMA were not varied. Permeability values are in square meters.

the caldera is forced to move laterally out to the flanks by the low permeabilities below the caldera fill. Subsequent to construction of the model, data from drill holes GEO N-1 and GEO N-3 confirmed our assumption that permeabilities are relatively high to depths of more than a kilometer on the flanks of the volcano. In core from GEO N-1, permeability decreases due to the presence of clays and fracture filling (T. Keith, oral communication, 1986) over an interval that corresponds to the lower part of model unit FLOW 2. At GEO N-3, recharge probably penetrates to depths between 900 and 1000 m and migrates laterally in a few permeable layers [*Swanberg et al.*, this issue]. The depth of penetration includes model unit FLOW 1 and most of FLOW 2.

The magma is assumed to be rhyolitic and to have a density of 2500 kg m^{-3} [*Clark*, 1966] and a constant thermal conductivity of 1.88 W m^{-1} K^{-1} [*Peck*, 1978; *Stout and Piwinskii*, 1980]. It is given a specific heat of 1.25 kJ kg^{-1} K^{-1} at temperatures below the solidus (assumed to be 800°C) [*Peck*, 1978; *Stout and Piwinskii*, 1980]. In early simulations the specific heat was set at 5.44 kJ kg^{-1} K^{-1} at temperatures above the solidus, in order to accommodate the latent heat of crystallization (270 kJ kg^{-1} [*Harris et al.*, 1970]) over a temperature range of 50°C between the initial temperature of 850°C and the solidus. In these early simulations the magma body was largely crystallized after 5000 years. Magmatic cooling rates in these simulations were similar to the results of *Blackwell and Steele* [1983], who also treated the magma body as an isolated, instantaneous source.

In our final simulations, from which most of the results presented here are derived, the specific heat of the magma was set at 16.0 kJ kg^{-1} K^{-1} at temperatures above the solidus. This is near the minimum level required to maintain magmatic temperatures above or near the solidus over a 10,000-year period. In this way, the model mimics the addition of heat to the magma by magmatic convection or basaltic underplating as suggested by *MacLeod and Sherrod* [this issue].

Ring dikes (DIKE) are represented as conduits having relatively high vertical permeability and relatively low horizontal permeability. An additional vertical feature (PIPE) represents a permeable conduit such as that formed by breccia and rubble in a cooled volcanic vent. The vent is placed beneath the Central Pumice Cone, but it could equally well represent a conduit beneath the Big Obsidian Flow, the youngest flow in the caldera (1350 B.P.) and the one nearest the Newberry 2 and RDO-1 test holes (Figure 2). The DIKES and PIPE allow exchange of fluid between the caldera-fill deposits and deep high-temperature zones. At Newberry there is no direct evidence that zones of enhanced vertical permeability are associated with the ring dikes and volcanic vents. However, permeable vertical conduits must exist somewhere in the caldera in order to convey thermal fluid to the shallow depths at which it was found in Newberry 2 and RDO-1. At Meager

TABLE 2. Rock and Fluid Properties Assigned to Each Material

Material Name	Density of Solid, kg m^{-3}	Effective Porosity	Thermal Conductivity, Solid/Liquid Mixture,* W m^{-1} K^{-1}	Specific Heat, Solid,* kJ kg^{-1} K^{-1}	Specific Heat, Fluid,† kJ kg^{-1} K^{-1}	Matrix Compressibility, Pa^{-1}
FILL	2700	0.25	0.85	1.00	4.2	5×10^{-10}
DIKES and PIPE	2700	0.15	1.66	1.00	4.2	5×10^{-10}
FLOW 1	2700	0.10	0.85	1.00	4.2	5×10^{-10}
FLOW 2	2700	0.075	1.66	1.00	4.2	5×10^{-10}
FLOW 3	2700	0.05	1.66	1.00	4.2	5×10^{-10}
FLOW 4	2700	0.01	1.66	1.00	4.2	5×10^{-10}
FLOW 5	2700	0.05	1.66	1.00	4.2	5×10^{-10}
MAGMA	2500‡	0.01	1.88	5.40§ or 16.0¶ (800°–850°C) 1.25 (001°–799°C)	4.2	5×10^{-10}

**Lachenbruch and Sass* [1977], *Peck* [1978], and *Stout and Piwinskii* [1980].

†Additional fluid properties were calculated by the computer program at each cycle as functions of pressure and temperature: fluid density, dynamic viscosity, fluid compressibility, and thermal expansivity.

‡*Clark* [1966].

§Includes latent heat of crystallization (270 kJ kg^{-1} [*Harris et al.*, 1970]).

¶Arbitrary value used in final simulations to maintain magma temperatures near 800°C over a 10,000-year period.

Mountain, near the northern end of the Cascade Range, drill hole data show that dikes and breccia zones are important in focusing upward movement [*Adams and Moore*, 1987].

The placement of PIPE illustrates a basic aspect of the model construction in that no attempt was made to model all of the vents, dikes, and faults that may be associated with specific surface features of the caldera. To do so would have presumed too much in view of our sparse knowledge of subsurface conditions. Rather, the goal was to model representative features and to extrapolate from the observed effects, at least qualitatively.

Permeabilities assigned to DIKE and PIPE were intended to be sufficiently high that they would not be a limiting control on the interchange of fluid between upper and lower zones of the model. The vertical permeability was set at 2.5×10^{-11} m^2 in the current models. Trials with higher values in previous models showed no significant effects on flow patterns and little effect on the flow rates.

Initial Conditions

The initial conditions for the cross-sectional model were a hydrostatic pressure distribution and the temperature distribution derived from 100,000 years of conductive cooling of a large intrusion within a radial model (Figure 4*b*). The simulations begin with the emplacement of another, relatively small, magma body near the top of the older body (Figure 4). This relatively small body represents the source of the Holocene eruptive cycle.

The initial temperature distribution is necessarily arbitrary but seems reasonable based on available geologic and geochemical information. The construction of the main edifice and collapse of the summit were clearly episodic processes interspersed with long periods of quiescence. Most of the mafic magma emplaced beneath the volcano during the past few hundred milennia had cooled and solidified prior to the silicic eruptive activity of the past 10,000 years. It must be assumed that hydrothermal systems existed during the construction of the volcano, but such systems would have dissipated much of their heat during the long quiescent periods. There is no evidence in the rocks sampled thus far, either on the flanks or beneath the caldera, that hydrothermal activity has ever been more intense or more extensive than it is at present [*Keith and Bargar*, this issue]. All of the geochemical and geophysical evidence points to a young, evolving hydrothermal system. This expanding hydrothermal system is interacting with large volumes of cold-water recharge.

Within the caldera, initial temperatures are cooler than those measured in the caldera drill holes. The initial temperature gradients on the flanks are similar to those measured in the lower parts of GEO N-1 and GEO N-3. We believe that the current hydrothermal system could reasonably be assumed to have developed during the past 10,000 years from a range of conditions similar to our initial conditions.

Patterns and Rates of Flow

The pattern of fluid circulation in this model differs in some details from those shown in classic modeling studies of groundwater circulation around cooling magma bodies, such as those of *Norton and Knight* [1977] and *Cathles* [1977]. These earlier studies involve systems with horizontal upper boundaries in which fluid circulation is driven solely by differences in fluid density caused by heating. At Newberry, the topographic relief of the water table has a strong influence on the potential field, tending to drive flow away from the center of the model.

The general pattern of flow is well established within a few hundreds of years after the magma is introduced. Except in the region above the magma, the flow pattern remains fairly constant over the 10,000-year period of our simulations and is nearly independent of the absolute values of permeability in the model, although rates of flow are not. In Figure 5, arrows denoting flow directions are scaled by fluid velocities for a simulation time of 10,000 years. Only the two extreme permeability cases are shown. Flow vectors in the intermediate-permeability case are generally smaller than but similar in direction to those in the high-permeability case.

Expansion of fluid in the vicinity of the magma causes fluid to move upward and outward away from the magma chamber at flow rates that are higher than those in the rest of FLOW 3. The upflow of thermal fluid is concentrated in the PIPE. Flow rates in the deeper parts of the system tend to decrease with time as the magma cools. In the high-permeability case, there is recirculation of cooler water in the direction of the magma body at depths of 2 km or more beneath the caldera. In the low-permeability case this convection cell is not as well developed. The difference in water table elevation from south to north does not cause significant asymmetry in the flow pattern, although temperatures differ between the north and south flanks. The major source of asymmetry in the flow pattern is the location of the PIPE, which is offset 1 km north of the caldera center.

Recharge enters the caldera surface and moves rapidly through the caldera-fill deposits. Little of the recharge moves directly downward except through the DIKES which, in all cases, serve as conduits for the cold recharge water. No more than 30% of the total recharge moves down the DIKES, however, and the bulk of the recharge moves laterally into FLOW 1. Most of the recharge then moves through FLOW 1 and FLOW 2 toward the side boundaries, where it leaves the system. In all cases, the cold, dense recharge water in the DIKES moves out into adjacent formations at slow rates. Except in the DIKES and PIPE, fluid circulation between the caldera fill and underlying zones is negligible.

Experiments with the cross-sectional model and with the earlier radial model show that recharge from outside the volcano cannot occur at the depths used in our models. The high water table in the caldera drives water away from the center of the model except in the convection cells that develop directly beneath the caldera. The lateral extent of inflow toward the magma increases with depth as density-related effects become increasingly significant.

The vector diagrams of Figure 5 illustrate the effect of permeability on the extent of lateral inflow for the low- and high-permeability cases at 10,000 years. The maximum lateral extent of inflow in the high-permeability case was about 10 km. In the intermediate-permeability case (not shown), lateral inflow occurred from a radius of 8–9 km, while in the low-permeability case (Figure 5), the only lateral inflow was that directed toward the PIPE from a distance no greater than a few kilometers.

It is possible that lateral recharge to the deep system from a regional water body could occur at depths well below the top of the magma, provided that permeabilities in the deeper rocks are sufficiently high. It is likely, however, that most recharge now occurs on the volcano itself.

In all of the cases considered and throughout the 10,000-year period of the simulations, mass discharge through the side boundaries slightly exceeded the rate of meteoric recharge in the caldera. Thus the total mass of fluid decreased slowly. The cause is primarily the volumetric expansion of water associated with heating; it implies that the system as the whole

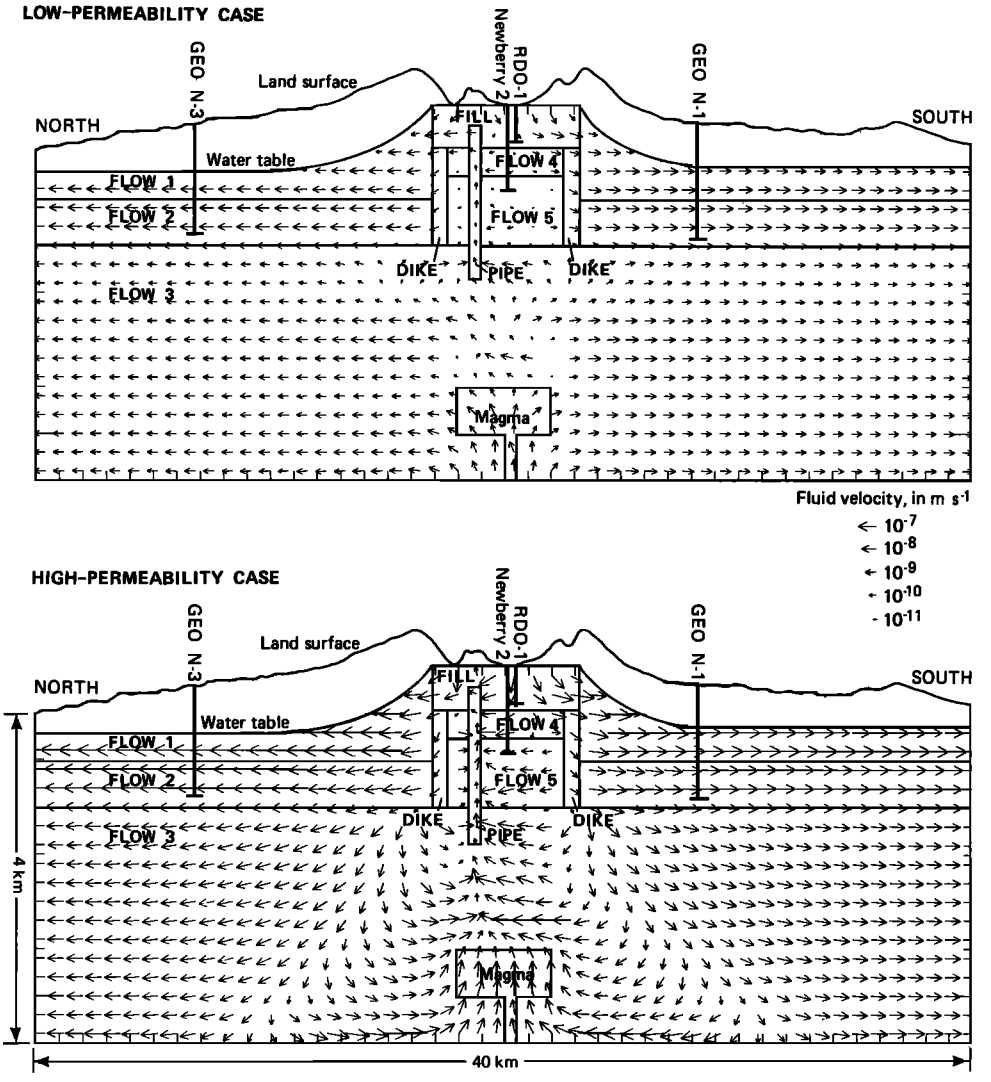

Fig. 5. Generalized patterns of flow in the cross-sectional model in the high- and low-permeability cases at a simulation time of 10,000 years. Arrows showing directions of fluid flow are scaled by fluid velocities.

is still warming at a time of 10,000 years. The trend would eventually reverse as the magma continues to cool.

Several sets of experiments were done to test the sensitivity of model results to changes in the permeability of a single material. These experiments showed that the rate of recharge in the caldera is particularly sensitive to permeability and anisotropy in the flank rocks (FLOW 1). Recharge rates ranged from 1.2×10^{-7} kg s^{-1} m^{-2} in the low-permeability case to 4.0×10^{-5} kg s^{-1} m^{-2} in the high-permeability case. Recharge in the caldera in the intermediate-permeability case was 6.4×10^{-6} kg s^{-1} m^{-2}, or within about 10% of *Sammel and Craig*'s [1983] budget estimate of 250 kg s^{-1}. The permeability values chosen for FLOW 1 in the intermediate-permeability case appear to be reasonable estimates of actual overall permeabilities on the flanks of the volcano.

Temperatures

Simulated temperature profiles at key locations and selected times are shown in Figure 6, together with the temperature profiles from Newberry 2 and GEO N-1. The drill holes can be located in Figure 4*a*.

In the low-permeability case, temperature changes in most of the nodes were small, less than 2°C in 10,000 years. Larger changes occurred in areas near the magma (Figures 6*b* and 6*c*) due to conductive heating, and in the DIKES and PIPE (Figures 6*a* and 6*b*), due to convection. In the PIPE, temperatures increased as much as 40°C in 10,000 years. At a depth of 875 m below the caldera surface, for example, the temperature is 180°C. For comparison, the temperature in Newberry 2 was about 230°C at this depth. Temperatures in FLOW 3 above the magma and at many nodes in the caldera were still increasing slowly after 10,000 years.

At 10,000 years, temperatures in the magma chamber have decreased from the initial value of 850°C to values approaching or below the solidus (795°–829°C). Temperature changes at representative nodes during the 10,000-year simulation period are shown in Figure 7.

In the intermediate-permeability case, in which recharge was close to the estimated value and all three of the vertical conduits showed a downward flow of cold recharge water, large temperature changes occurred in parts of the upper 1.5 km of the model. The maximum changes were 85°–90°C decreases in the ring fractures (DIKES) that resulted from the recharge of meteoric water. Temperatures in the deep nodes of

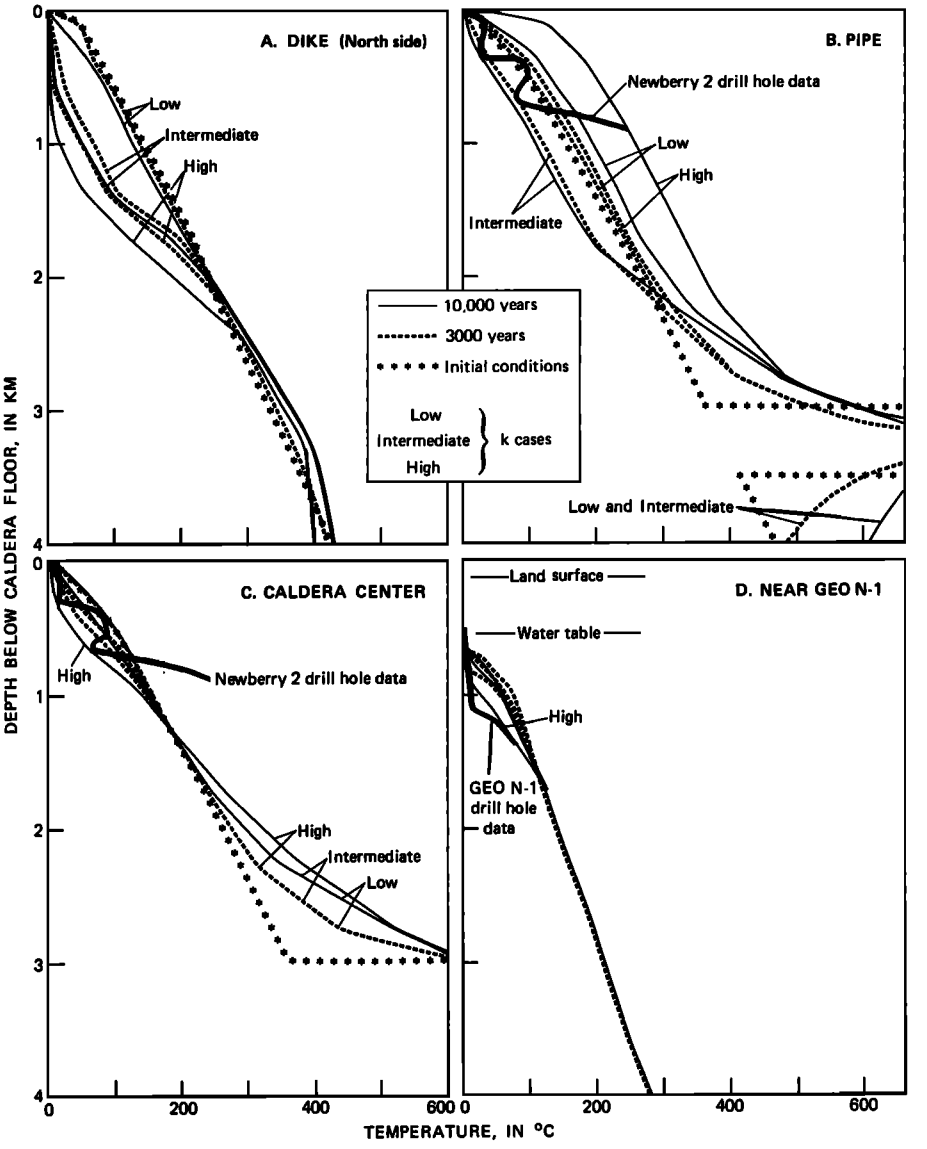

Fig. 6. Temperature profiles at selected locations at times of 3000 and 10,000 years in the low-, intermediate-, and high-permeability cases. Locations of Newberry 2 and GEO N-1 are shown in Figure 4.

FLOW 3 and MAGMA were similar to those in the low-permeability case (Figure 7).

The agreement, noted above, between simulated recharge rates in the intermediate-permeability case and those estimated by *Sammel and Craig* [1983] suggests that the permeabilities of FILL and FLOW 1 in this case are reasonable choices. However, comparison of the model temperatures with profiles measured in GEO N-1 (Figure 6*d*) and GEO N-3 (not shown) suggests that vertical permeability in the flank rocks may be locally higher than that used in the intermediate case.

In the high-permeability case, the rate of the flow up the PIPE was relatively high, and temperatures in the PIPE were greater than in the other cases as a result. At 10,000 years, the temperature in PIPE at a depth of 875 m below the caldera surface was 245°C, or about 3° higher than the temperature in Newberry 2 at the same depth (Figure 6*b*).

Our results differ from those of *Blackwell and Steele* [1983] in terms of rates of heating in the region above the magma. In general, the upward movement of the thermal front in the model of Blackwell and Steele is faster than that in our model because of the higher permeability in their model. However, within and below the PIPE in our model, the rates of heating can be higher. For example, at a time of 10,000 years, temperatures about 1 km above the magma have increased 100°C in Blackwell and Steele's model, while a temperature increase of 100°C occurs in the PIPE almost 3 km above the magma and only 125 m below land surface in our high-permeability case.

Temperatures in the magma at 10,000 years in the high-permeability case (range 792°–829°C) are nearly the same as those in the low and intermediate cases (range 795°–829°C). The similarity indicates that heat conduction, rather than convection, controls magmatic cooling in each case despite a 2–3 order-of-magnitude difference in permeability in the adjacent rocks (Table 1). By analogy to the results of *Norton and Knight* [1977], we attribute our results to the low permeability of the magma itself. This conclusion is supported by the fact that the convection that occurs in FLOW 3 in our high-permeability case is not reflected in significant temperature

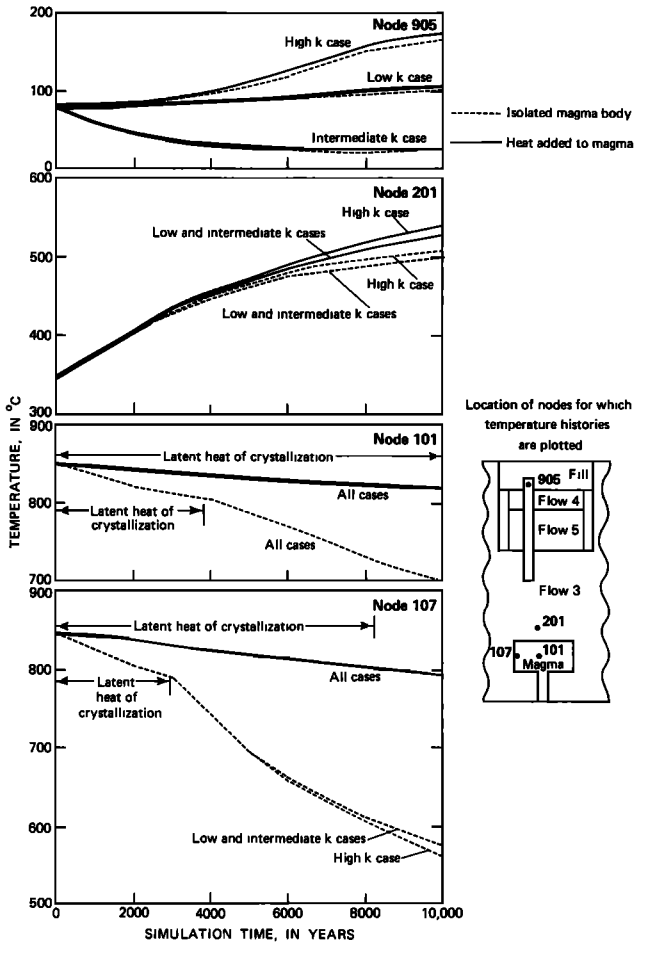

Fig. 7. Change in temperature with time at selected locations in the low-, intermediate-, and high-permeability cases. This figure also illustrates the effects of simulating the addition of heat to the magma, versus treating the magma as an isolated body. The added heat has little effect on temperatures except very near the magma body, but does keep magmatic temperatures above or near 800°C over the 10,000-year period simulated. When the magma is treated as an isolated body, it is largely crystallized within 5000 years.

differences in the magma compared with the lower-permeability cases. The low permeability assigned to the magma probably is appropriate to its noncrystalline state.

Heat Flow

In the low- and intermediate-permeability cases, the vertical flow of heat is dominantly conductive in all regions of the models except in the caldera-fill deposits, DIKES, and PIPE. In the high-permeability case, vertical heat transport is dominated by convection except in FLOW 4 and FLOW 5. Lateral heat transport is predominantly convective in all three cases.

Heat transfer by conduction. The heat flows observed at shallow depths in the model at a simulation time of 10,000 years may be compared with apparent heat flows observed in drill holes Newberry 2, GEO N-1, and GEO N-3. Vertical heat flows at selected model locations are given in Table 3.

Conductive heat flow through the bottom of the caldera-fill deposits (Figure 4*a* and Table 3) ranged from 160 mW m^{-2} to 230 mW m^{-2} in the low-, intermediate-, and high-permeability cases. Conductive heat flow through the base of FLOW 5, at a depth of 1.5 km, ranged from 205 to 260 mW m^{-2}. These values are considerably lower than the heat flows that have been estimated from the temperature profile from Newberry 2. A discussion of these differences is in order.

Temperatures measured in the lower 180 m of Newberry 2 (Figure 8) were the basis for an earlier estimate that conductive heat flow through this interval is as high as 1100 mW m^{-2} [*MacLeod and Sammel*, 1982]. However, close examination of the data for this interval shows that the profile is far from linear, and it is clear that the temperature profile is either a transient one, or has convective components, or both. The bottom 80 m of the profile is nearly linear and has a temperature gradient of about 500°C km^{-1} which, combined with a harmonic mean thermal conductivity of 1.76 W m^{-1} K^{-1} obtained from six measurements on core from this interval (R. J. Munroe, written communication, 1986), gives a calculated heat flow of about 880 mW m^{-2}. Even this segment of the profile has minor convective perturbations, however.

Above the predominantly conductive zone seen in the Newberry 2 profile, in the depth interval 550–675 m, temperatures of 75°–77°C occur in dacitic breccias and pumiceous sediments. This cool-water zone constraints the upper end of the quasi-linear profile and, together with the high-temperature convective zone at a depth of 930 m [*Keith and Bargar*, this issue], imposes the high-temperature gradients observed in the lower 270 m of the hole. If heat were not being efficiently removed by convection in the rocks above 675-m depth, the temperature gradient between the hole bottom and land sur-

TABLE 3. Vertical Heat Flow Observed in the Model at 10,000 Years Simulation Time

Location and Depth	Heat Flow, mW m^{-2}		
	Low-*k* Case	Intermediate-*k* Case	High-*k* Case
Below Caldera Fill			
Between FLOW 4 and FILL (500 m below land surface)	−160 (−<1)	−210 (+105)	−230 (−3900)
Between FLOW 3 and FLOW 5 (1. 5 km below land surface)	−205 (−15)	−260 (+80)	−225 (−1900)
Area Near Drill Hole GEO N-1			
Between FLOW 2 and FLOW 1 (830 m below land surface)	−135 (+1)	−200 (−44)	−220 (+21)
Midpoint of FLOW 2 (1080 m below land surface)	−130 (+1)	−160 (−34)	−215 (+58)
Between FLOW 3 and FLOW 2 (1330 m below land surface)	−125 (−<1)	−105 (+<1)	−180 (−105)
Area Near Drill Hole GEO N-3			
Between FLOW 2 and FLOW 1 (830 m below land surface)	−105 (−<1)	−105 (−12)	−200 (+1)
Midpoint of FLOW 2 (1053 m below land surface)	−105 (−<1)	−90 (−8)	−155 (+13)
Between FLOW 3 and FLOW 2 (1303 m below land surface)	−105 (−<1)	−80 (+<1)	−110 (+48)

Values are conductive heat flow. Values in parentheses are convective heat flow. Negative values indicate upward flow. See Figure 4 for locations referred to.

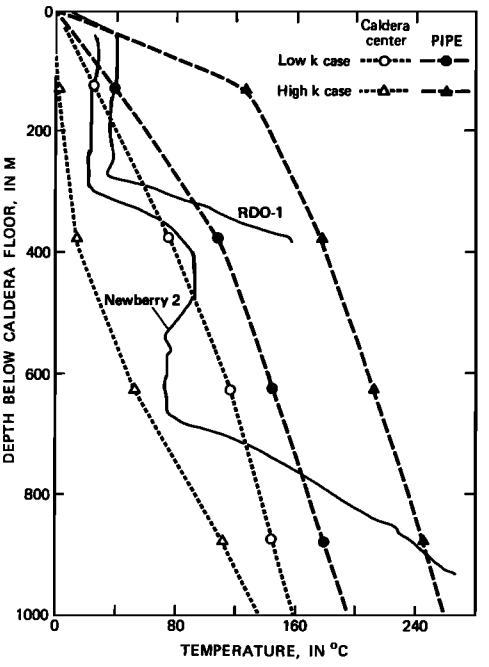

Fig. 8. Comparison between measured temperatures from Newberry 2 and RDO-1 and simulated temperatures in the PIPE and near the caldera center at a simulation time of 10,000 years.

face would be about 285°C km^{-1}, and the conductive heat flow would be about 320 mW m^{-2}.

In our high-permeability case, simulated temperatures are high enough in the PIPE and low enough outside the PIPE that a profile similar to Newberry 2 could be generated in our model by adding horizontal stratification within the FILL and FLOW 3 (see Figure 8). However, this addition would require a finer node network than is warranted by current information; we have no knowledge of the details of the permeability structure.

On the right side of the model (south flank of Newberry), simulated conductive heat flows at locations and depths corresponding to those of drill hole GEO N-1 range from 105 to 220 mW m^{-2}. Heat flow in GEO N-1 was calculated as an average of 180 mW m^{-2} for the depth interval 1164–1219 m [*Swanberg et al.*, this issue]. This interval corresponds best to the middle of FLOW 2 (1080 m below land surface), where heat flow in the model ranged from 130 to 215 mW m^{-2} in the three permeability cases. The value cited by Swanberg et al. is best matched by the figure in our intermediate-permeability case (160 mW m^{-2}).

In the vicinity of GEO N-3, conductive heat flows in the model ranged from 80 to 200 mW m^{-2}. Heat flow calculated for the depth interval 1170–1220 m in GEO N-3 was 86 mW m^{-2} [*Swanberg et al.*, this issue]. In the model interval that includes these drill hole depths, heat flow in the intermediate-permeability case (90 mW m^{-2}) again is the best match to the field data.

At shallow depths on three sides of the volcano, temperatures in drill holes GEO N-1, GEO N-3, and Newberry 1 (Figure 2) were low, profiles were nearly isothermal, and heat flows apparently were extremely small. This phenomenon is caused by lateral and vertical flow of cold meteoric water and is common at relatively shallow depths in the High Cascades and in the High Lava Plains northwest of Newberry [*Blackwell et al.*, 1982; S. E. Ingebritsen, unpublished data, 1987]. The isothermal zone on the flanks is best developed in the high-permeability case.

In general, simulated conductive heat flows in regions corresponding to the lower parts of GEO N-1 and GEO N-3 increase with permeability in our model (Table 3). However, examination of the temperature profiles on the flanks (e.g., Figure 6*d*) shows that this reflects the development of the isothermal zone, rather than higher temperatures at depth. The elevated temperature gradients measured in the lower portions of GEO N-1 and GEO N-3 are probably not related to the postulated Holocene magma body. They are more likely related to the cumulative effect of older intrusions (represented by the initial conditions) and may be steepened by the overlying isothermal zone.

Heat transfer by convection. The Rayleigh number is an indicator of the potential for free convection due to buoyancy forces only. Rayleigh numbers evaluated for conditions in the central region of the model, i.e., fluid properties at mean temperatures and an overall temperature difference of 640°C between the bottom of FLOW 5 and the magma chamber, do not exceed the theoretical critical number for the onset of convective flow ($4\pi^2$) [*Lapwood*, 1948]. The Nusselt number may be defined as the ratio of total heat flow to heat flow by conduction only. Nusselt numbers calculated at central locations above the magma generally exceed 3 in the high-permeability case, indicating that convection accounts for 2–3 times as much heat flow as conduction. Any Nusselt number greater than 1, in conjunction with a Rayleigh number of 40 or less, indicates that forced convection is effective in driving the system and that classical free convection cells are either distorted or absent. (See *Sorey* [1978] for the relation between Rayleigh and Nusselt numbers.)

Nearly all of the vertical convective heat transport between the caldera fill and deep high-temperature zones occurs in the DIKES and PIPE. In the low- and intermediate-permeability cases, heat transfer between these regions was dominantly conductive at a simulation time of 10,000 years; in the high-permeability case it was dominantly convective (Table 3). In the high-permeability case, upward convective heat flow in the PIPE was 23.9 W m^{-2} at the level of the contact between FLOW 3 and FLOW 5, and 49.2 W m^{-2} between FLOW 4 and FILL. However, downward flow in the DIKES was also high, so that the net convective heat flow was 1.9 W m^{-2} and 3.9 W m^{-2} at these two depths (Table 3).

On the flanks of the model, vertical convective heat flow was relatively low and less affected by changes in permeability (Table 3). At depths less than about a kilometer, convective heat flow was upward in the intermediate case and downward in the high-permeability case. At depths of about 1300 m, convective flow was negligible in the intermediate case, and in the high-permeability case was upward on the south flank near GEO N-1 and downward on the north flank near GEO N-3.

The model results thus differ in detail from conditions in the drill holes, where artesian flow was reported in GEO N-3 and none was reported in GEO N-1 [*Swanberg et al.*, this issue]. Nevertheless, the general effect of cold meteoric recharge, referred to as "the rain curtain," is well reproduced by the model. The so-called rain curtain lowers simulated temperatures on the flanks of the mountain to depths of at least a kilometer in the high-permeability case, even in the absence of meteoric recharge on the flanks (Figure 6*d*). The effects of meteoric recharge on the temperature distribution extend to

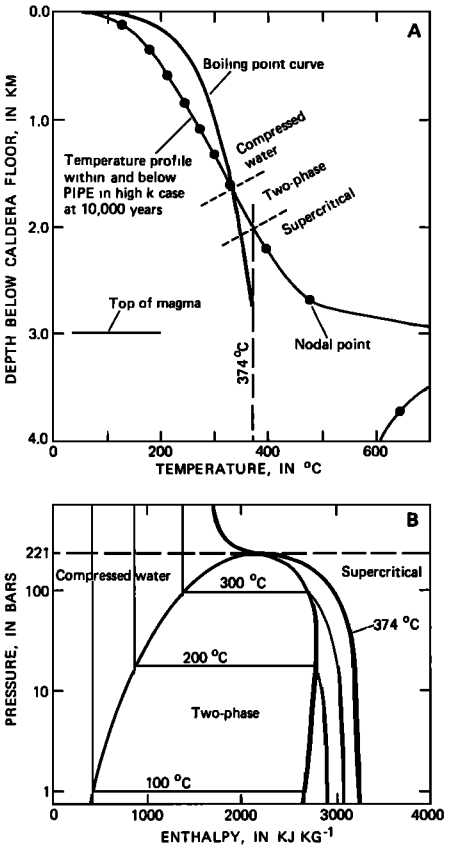

Fig. 9. (*a*) Temperature profile within and below the PIPE in the high-permeability case at 10,000 years, relative to a boiling point curve and the critical temperature (374°C). Nodes immediately above the magma are at supercritical temperatures; overlying nodes are in the compressed liquid region. A two-phase zone is inferred but would not be intercepted by any of the nodal points. (*b*) Pressure/enthalpy diagram for pure water and vapor, showing the compressed water, two-phase, and supercritical regions. The top of the two-phase envelope is at a pressure of about 221 bars, or a hydrostatic depth of 2.2 km.

depths of more than 2 km near the DIKES in the high-permeability case (see, e.g., Figure 6*b*).

The cooling effects of recharge are greater on the north flank than on the south flank of the model, a result consistent with the 16°C temperature difference between GEO N-1 and GEO N-3 at maximum comparable depths (at an elevation of 560 m, or depths of 1220 and 1190 m in GEO N-1 and GEO N-3, respectively [*Swanberg et al.*, this issue]). The asymmetrical cooling pattern on the flanks probably is due to the difference in water table elevation between the south and north sides of the mountain, which produces a slight excess of cold-water flow toward the northern boundary. The possibility of this outcome was anticipated in the decision to employ an assymetrical cross-sectional model.

Two-Phase Conditions

The initial pressure and temperature conditions in the model are such that the fluid throughout the system is a single-phase liquid. Following the emplacement of the magma, we would expect supercritical and, possibly, two-phase zones to develop above the magma. The development of a two-phase zone would be enhanced by high permeabilities in FLOW 3, which would allow pressures to drop below initial levels as the fluid above the magma is heated. Lower permeabilities in FLOW 3 would slow pressure drops by inhibiting the movement of heated fluid. (An extremely low permeability, i.e., lower than those considered, would lead to thermal pressurization above the magma.)

The presence of a two-phase zone above the magma body is implicit in some of our results. The inferred two-phase zone would be thickest below the PIPE at late times in the high-permeability case; however, even in this case the zone is not thick enough to be detected directly in the numerical solution. That is, it is thin enough to fall between two nodal points (Figure 9*a*). The temperature profile in Figure 9*a* shows supercritical temperatures immediately above the magma body, with a transition to single-phase liquid (compressed water) through the inferred two-phase zone. In general, supercritical and two-phase conditions are found in the model only within 1 km of the magma body.

The two-phase zone probably would not significantly increase the net transfer of heat away from the magma, as magmatic heat loss was conduction dominated in our simulations, but we would expect temperatures in the two-phase region to fall along the boiling-point-with-depth curve (Figure 9*a*) if two-phase conditions were included in the calculations and the grid were finer. The presence of significant quantities of CO_2 at depth at Newberry (as shown by the flow test data) would tend to expand any two-phase zone relative to a pure water system [e.g., *O'Sullivan et al.*, 1985].

CONCLUSIONS

The availability of geological and geophysical data at Newberry, the radial symmetry of the volcano, and its isolation from other eruptive centers make Newberry relatively well suited for hydrologic modeling. Though uncertainties regarding the permeability structure and appropriate initial conditions make our model nonunique, several fairly general conclusions can be drawn.

Simulated temperatures in and below the caldera fill to a depth of more than a kilometer are highly sensitive to the magnitude of recharge to the caldera, which in turn is sensitive to the permeability of the rocks surrounding the caldera. The model results suggest that the average permeabilities of the caldera-fill deposits and adjacent flank rocks may be similar to those used in our intermediate permeability case.

Simulated recharge at a rate of about 250 kg s^{-1}, which corresponds to an estimate of the actual recharge, cools large volumes of the caldera-fill units to temperatures well below those observed in Newberry 2 and RDO-1. These cooler temperatures correspond to temperatures observed in water wells in the caldera. Much higher temperatures occur in the model, however, near upflow conduits that bring thermal water close to the surface. Both Newberry 2 and RDO-1 are located less than 1 km from fumarolic vents, less than 2 km from the vent of the Big Obsidian Flow (the most recent eruptive feature in the caldera), and less than 1 km from an inner ring fracture zone. The model results indicate that hot water found in the two test holes could have risen in permeable channels associated with one or more of these features.

In the deeper regions of the model, permeabilities used in our high-permeability case may correspond best to actual values because these higher permeabilities permit thermal upflow at rates suggested by the data from Newberry 2 and RDO-1. The permeability of the conduits themselves is not a limiting factor in our models.

Simulated temperatures on the flanks of the volcano decrease from the conduction-only initial conditions due to outward and downward movement of recharge from the caldera.

The elevated temperature gradients measured in the lower portions of the drill holes on the flanks are probably related to the cumulative effect of older intrusions, rather than the postulated Holocene magma body. Simulated gradients at these locations increase with permeability in our model, due to the thickening of the overlying isothermal zone.

Buoyancy forces caused by thermal expansion are the principal driving mechanism in the region of the model close to the magma. However, high Nusselt numbers calculated for this region, in conjunction with low Rayleigh numbers, indicate that forced convection is also important. Elsewhere in the system, directions of flow are largely controlled by the mounding of the water table below the caldera. Lateral flows beneath the flanks of the volcano are driven by topography.

Most recharge that reaches the deep hydrothermal system must originate on the volcano itself. Lateral recharge from outside the volcano could occur only at great depth due to the high water table below the caldera. Convection cells that develop at depths 2–3 km below the caldera surface are sensitive to the recharge in the caldera as well as to permeabilities in the deeper rocks.

Flow velocities were low in most regions, even in the high-permeability case. Recharge water from the caldera might reach the outer boundary of the model in about 6000 years at an average fluid velocity of 3 m/yr. In the deeper regions beneath the caldera, however, velocities in the model are much slower. An implication of these observations is that the use of isotopes (such as deuterium) to deduce locations of recharge areas and the provenance of thermal fluids may be difficult, in that at least a significant fraction of the water may have been recharged in the Pleistocene.

The temperature at a depth of 930 m in an upflow zone of the high-permeability model is close to the maximum temperature in Newberry 2. However, as we noted in the discussion of heat flow, the model does not reproduce the high-temperature gradients that were measured in Newberry 2 between the depth of about 680 m and the bottom of the hole at 932 m. The reason for the unexceptional temperature gradient above this depth in the model is the lack of a stratum of cooler water comparable to that found in Newberry 2 between depths of 550 and 675 m. The permeability structure in the caldera fill is undoubtedly highly complex and it is unknown in most of the caldera. These considerations resulted in the decision to maintain generality in the model rather than to mimic closely the details known only in one region of the caldera.

In connection with the temperature gradient measured in Newberry 2, it may be worth noting that the temperatures obtained below a depth of 760 m were bottom-hole measurements made as drilling progressed. There can be no assurance as to the long-term stability of the temperature profile and the calculated heat flow from these depths.

The model demonstrates that high temperatures can be maintained at depths comparable to those penetrated by Newberry 2 (less than 1 km) by means of areally restricted upflow from a zone of convection that overlies a much deeper magma chamber. Permeable conduits are required in order to permit water and heat to penetrate the overlying caprock in large quantities. Though the temperature gradient observed in the bottom 80 m of Newberry 2 projects to magmatic temperatures at a depth of about 2.1 km, a convecting zone overlying a magma body at a depth of about 3 km appears to be the more likely possibility in the light of the most recent interpretation of seismic data [*Achauer et al.*, this issue].

APPENDIX

The single-phase geothermal simulator used in this study, PT, is documented by *Bodvarsson* [1982]. The PT code uses the integrated finite-difference method to solve numerical approximations to mass and energy balance equations which can be written

$$\int_V \frac{\partial}{\partial t}(\phi\rho)\,dV = -\int_A \rho \mathbf{v}_d \cdot \mathbf{n}\,dA + \int_V G_f\,dV$$

and

$$\int_V \frac{\partial}{\partial t}(\rho_m e)\,dV = \int_A \lambda \nabla T \cdot \mathbf{n}\,dA - \int_A \rho c_f\,\delta T \mathbf{v}_d \cdot \mathbf{n}\,dA + \int_V G_h\,dV$$

respectively [*Bodvarsson*, 1982], where t is time, ϕ is effective porosity, ρ and ρ_m are density of the fluid and the medium, respectively, V is volume, $\mathbf{v}_d$ is specific discharge, $\mathbf{n}$ is a unit vector normal to an interface, A is area, e is internal energy of the medium, λ is medium thermal conductivity, T is temperature and δT denotes an interface temperature, c_f is the isovolumetric heat capacity of the fluid, and G_f and G_h are mass and heat source/sink terms, respectively.

Specific discharge (Darcy velocity) is calculated using Darcy's law. The mass and energy balance equations are coupled through pressure- and temperature-dependent parameters, as well as the convective terms.

The thermodynamic range of the code (originally to 400 bars, 350°C) was increased by fitting a bicubic spline to the water-density data of *Keenan et al.* [1978], with pressure and temperature as the independent variables; and by fitting a polynomial surface to the viscosity data of Keenan et al. Bicubic splines preserve continuity through the second derivative, so that the spline approach allows fluid compressibility and expansivity to be calculated readily as partial derivatives. The modified code still treats the heat capacity of the fluid as a constant. Over most of the thermodynamic range modeled, fluid heat capacity varies only between about 3.0 and 6.4 kJ kg^{-1} K^{-1}. However, heat capacity increases dramatically in the critical region. This would cause fluid heat transport properties to be enhanced in a thin zone above the magma. To adequately represent critical region phenomena would require a finer node network than that used in our models, as well as an accurate description of $c_f(P, T)$. Consider, for example, Figure 9*a*. At the nodal point below the critical isotherm (374°C), $c_f(P, T)$ would be about 3.5 kJ kg^{-1} K^{-1}; at the nodal point above the critical isotherm, it would be about 5.3 kJ kg^{-1} K^{-1}. Though $c_f(P, T)$ would be very high at the two-phase supercritical boundary, the high-c_f zone would be thin enough that it would be essentially "overlooked" in the numerical solution in this case.

We do not believe that treating c_f as a variable function would significantly affect the flow and temperature fields at the generalized scale considered. Errors introduced by treating c_f as a constant are probably small relative to the uncertainties in the values assigned to rock properties. Similarly, we do not believe that the thin two-phase zone inferred to be present at later times in the high-permeability case would significantly affect our conclusions. However, we plan to reconsider these problems with a code that describes $c_f(P, T)$ accurately and has two-phase capabilities, in order to evaluate these assumptions.

Acknowledgments. The authors are grateful to a number of colleagues in the U.S. Geological Survey for help and support made available during this study, and in particular to Michael Sorey, Allen Moench, Terry Keith, David Sherrod, and David Fitterman for constructive criticism of earlier versions of this report; and to David Jones for drafting the figures. We thank John Daggett of Lawrence Berkeley Laboratory, Earth Sciences Division, for producing the vector flow diagrams used in Figure 5.

REFERENCES

Achauer, U., J. R. Evans, and D. A. Stauber, High-resolution seismic tomography of compressional wave velocity structure at Newberry Volcano, Oregon Cascade Range, *J. Geophys. Res.*, this issue.

Adams, M. C., and J. N. Moore, Hydrothermal alteration and fluid geochemistry of the Meager Mountain geothermal system, British Columbia, *Am. J. Sci., 287*, 720–755, 1987.

Black, G. L., G. R. Priest, and N. M. Woller, Temperature data and drilling history of the Sandia National Laboratories Well at Newberry caldera, *Oreg. Geol., 46*, 7–9, 1984.

Blackwell, D. D., and J. L. Steele, Thermal model of the Newberry Volcano, Oregon, Survey of potential geothermal exploration sites at Newberry Volcano Deschutes County, Oregon, *Open File Rep. 0-83-3*, pp. 83–113, Oregon Dep. of Geol. Miner. Ind., Portland, 1983.

Blackwell, D. D., R. G. Bowen, D. A. Hull, J. Riccio, and J. L. Steele, Heat flow, arc volcanism, and subduction in northern Oregon, *J. Geophys. Res., 87*, 8735–8754, 1982.

Bodvarsson, G. S., Mathematical modeling of geothermal systems, Ph.D. thesis, Univ. of Calif., Berkeley, 1982.

Brace, W. F., Permeability of crystalline and argillaceous rocks, *Int. J. Rock Mech. Miner. Sci., 17*, 241–251, 1980.

Brace, W. F., Permeability of crystalline rocks: New in situ measurements, *J. Geophys. Res., 89*, 4327–4330, 1984.

Carothers, W. W., R. H. Mariner, and T. E. C. Keith, Isotopic composition of minerals and fluids from Newberry Volcano, Oregon, *J. Volcanol. Geotherm. Res., 31*, 47–63, 1987.

Cathles, L. M., An analysis of the cooling of intrusives by groundwater convection which includes boiling, *Econ. Geol., 72*, 804–826, 1977.

Clark, S. P., Jr. (Ed.), Handbook of physical constants, *Mem. Geol. Soc. Am., 97*, 93, 1966.

Fitterman, D. V., W. D. Stanley, and R. J. Bisdorf, Electrical structure of Newberry Volcano, Oregon, *J. Geophys. Res.*, this issue.

Griscom, A., and C. V. Roberts, Gravity and magnetic interpretation of Newberry Volcano, Survey of potential geothermal exploration sites at Newberry Volcano, Deschutes County, Oregon, *Open File Rep. 0-83-3*, pp. 68–81, Oreg. Dep. of Geol. and Miner. Ind., Portland, 1983.

Hardee, H. C., Permeable convection above magma bodies, *Tectonophysics, 84*, 179–195, 1982.

Harris, P. G., W. Q. Kennedy, and C. M. Scarfe, Volcanism versus plutonism—The effect of chemical composition, Mechanism of igneous intrusion, *Geol. J. Spec. Issue, 2*, 187–200, 1970.

Henley, R. W., and A. J. Ellis, Geothermal systems ancient and modern: A geochemical review, *Earth Sci. Rev., 19*, 1–50, 1983.

Ingebritsen, S. E., W. W. Carothers, R. H. Mariner, J. S. Gudmundsson, and E. A. Sammel, Flow testing of the Newberry 2 research drillhole, Newberry Volcano, Oregon, *U.S. Geol. Surv. Water Resour. Invest., 86-4133*, 1986.

Keenan, J. H., F. G. Keys, P. G. Hill, and J. G. Moore, *Thermodynamic Properties of Water, Including Vapor, Liquid, and Solid Phases*, John Wiley, New York, 1978.

Keith, T. E. C., and K. E. Bargar, Petrology and hydrothermal mineralogy of U.S. Geological Survey Newberry 2 drill core from Newberry caldera, Oregon, *J. Geophys. Res.*, this issue.

Lachenbruch, A. H., and J. Sass, Heat flow in the United States and the thermal regime of the crust, in *The Nature and Physical Properties of the Earth's Crust, Geophys. Monogr. 20*, edited by J. G. Heacock, pp. 626–675, AGU, Washington, D. C., 1977.

Lapwood, E. R., Convection of a fluid in a porous media, *Cambridge Philos. Soc., 44*, 508–521, 1948.

MacLeod, N. S., and E. A. Sammel, Newberry Volcano, Oregon: A Cascade range geothermal prospect, *Oreg. Geol., 44*, 123–131, 1982.

MacLeod, N. S., and D. R. Sherrod, Geologic evidence for a magma chamber beneath Newberry Volcano, Oregon, *J. Geophys. Res.*, this issue.

MacLeod, N. S., G. W. Walker, and E. H. McKee, Geothermal significance of eastward increase in age of upper Cenozoic rhyolitic domes in southeast Oregon, *Proc. U.N. Symp. Dev. Use Geotherm. Resour., 2nd, 1*, 465–474, 1975.

MacLeod, N. S., D. R. Sherrod, L. A. Chitwood, and E. H. McKee, Newberry Volcano, Oregon, Guide to some volcanic terranes in Washington, Oregon, and northern California, *U.S. Geol. Surv. Circ., 838*, 85–103, 1981.

MacLeod, N. S., D. R. Sherrod, and L. K. Chitwood, Geologic map of Newberry Volcano, Deschutes, Klamath, and Lake counties, Oregon, *U.S. Geol. Surv. Open File Rep., 82-847*, 1982.

Norton, D., and J. Knight, Transport phenomena in hydrothermal systems: Cooling plutons, *Am. J. Sci., 277*, 937–981, 1977.

O'Sullivan, M. J., G. S. Bodvarsson, K. Pruess, and M. R. Blakeley, Fluid and heat flow in gas-rich geothermal reservoirs, *J. Soc. Pet. Eng.*, 215–226, 1985.

Peck, D. L., Cooling and vesiculation of Alae Lava Lake, Hawaii, *U.S. Geol. Surv. Prof. Pap., 935-B*, 1978.

Priest, G. R., N. M. Woller, G. L. Black, and S. H. Evans, Overview of the geology of the central Oregon Cascade Range, Geology and geothermal resources of the Cascade Range, *Spec. Pap. 15*, pp. 3–28, Oreg. Dep. of Geol. and Miner. Ind., Portland, 1983.

Pruess, K., and T. N. Narasimhan, On fluid reserves and the production of superheated steam from fractured, vapor-dominated geothermal reservoirs, *J. Geophys. Res., 87*, 9329–9339, 1982.

Sammel, E. A., Hydrogeologic appraisal of the Klamath Falls geothermal area, Oregon, *U.S. Geol. Surv. Prof. Pap., 1044-G*, 1980.

Sammel, E. A., Results of test drilling at Newberry Volcano, Oregon, *Bull. Geotherm. Resour. Counc., 10*(11), 3–8, 1981.

Sammel, E. A., The shallow hydrothermal system at Newberry Volcano, Oregon: A conceptual model, *Trans. Geotherm. Resour. Counc., 7*, 325–330, 1983.

Sammel, E. A., and R. W. Craig, The geothermal hydrology of Warner Valley, Oregon: A reconnaissance study, *U.S. Geol. Surv. Prof. Pap., 1044-I*, 1981.

Sammel, E. A., and R. W. Craig, Hydrology of the Newberry Volcano caldera, Oregon, *U.S. Geol. Surv. Water Resour. Invest., 83-4091*, 1983.

Sorey, M. L., Numerical modeling of liquid geothermal systems, *U.S. Geol. Surv. Prof. Pap., 1044-D*, 1978.

Stauber, D. A., S. M. Green, and H. M. Iyer, Three-dimensional *P* velocity structure of the crust below Newberry Volcano, Oregon, *J. Geophys. Res.*, this issue.

Stout, N. D., and A. J. Piwinskii, The enthalpy (H_T-H_{298}) of anhydrous silicate melts from 1520–2600 K, *Rep. UCRL-52978*, Lawrence Livermore Lab., Berkeley, Calif., 1980.

Swanberg, C. A., W. C. Walkey, and J. Combs, Core hole drilling and the "rain curtain" phenomenon at Newberry Volcano, Oregon, *J. Geophys. Res.*, this issue.

Wells, F. G., and D. L. Peck, Geologic map of Oregon west of the 121st meridian, *U.S. Geol. Surv. Misc. Geol. Invest. Map, I-325*, 1961.

Williams, D. L., and C. Finn, Analysis of gravity data in volcanic terrain and gravity anomalies and subvolcanic intrusions in the Cascade Range USA and at other selected volcanoes, in *The Utility of Regional Gravity and Magnetic Anomaly Maps*, edited by W. J. Hinze, pp. 361–374, Society of Exploration Geophysicists, Tulsa, Okla., 1985.

S. E. Ingebritsen, R. H. Mariner, and E. A. Sammel, U.S. Geological Survey, 345 Middlefield Road, Menlo Park, CA 94025.

(Received April 24, 1987;
revised December 29, 1987;
accepted March 18, 1988.)